Role of Proinsulin Self-Association in Mutant *INS* Gene–Induced Diabetes of Youth

Jinhong Sun,[1] Yi Xiong,[1] Xin Li,[2] Leena Haataja,[1] Wei Chen,[1,3] Saiful A. Mir,[4] Li Lv,[2] Rachel Madley,[1] Dennis Larkin,[1] Arfah Anjum,[1] Balamurugan Dhayalan,[5] Nischay Rege,[6] Nalinda P. Wickramasinghe,[6] Michael A. Weiss,[5] Pamela Itkin-Ansari,[4,7] Randal J. Kaufman,[8] David A. Ostrov,[9] Peter Arvan,[1] and Ming Liu[1,2]

Diabetes 2020;69:954–964 | https://doi.org/10.2337/db19-1106

Abnormal interactions between misfolded mutant and wild-type (WT) proinsulin (PI) in the endoplasmic reticulum (ER) drive the molecular pathogenesis of mutant *INS* gene–induced diabetes of youth (MIDY). How these abnormal interactions are initiated remains unknown. Normally, PI-WT dimerizes in the ER. Here, we suggest that the normal PI-PI contact surface, involving the B-chain, contributes to dominant-negative effects of misfolded MIDY mutants. Specifically, we find that PI B-chain tyrosine-16 (Tyr-B16), which is a key residue in normal PI dimerization, helps confer dominant-negative behavior of MIDY mutant PI-C(A7)Y. Substitutions of Tyr-B16 with either Ala, Asp, or Pro in PI-C(A7)Y decrease the abnormal interactions between the MIDY mutant and PI-WT, rescuing PI-WT export, limiting ER stress, and increasing insulin production in β-cells and human islets. This study reveals the first evidence indicating that noncovalent PI-PI contact initiates dominant-negative behavior of misfolded PI, pointing to a novel therapeutic target to enhance PI-WT export and increase insulin production.

Proinsulin (PI) misfolding, endoplasmic reticulum (ER) stress, and decreased β-cell mass are key features of β-cell failure and diabetes in the autosomal-dominant diabetes known as mutant *INS* gene–induced diabetes of youth (MIDY) (1–3). All MIDY patients carry a mutation in only one of two *INS* alleles (3–6), and, in principle, one normal *INS* allele should be sufficient to maintain normoglycemia (7). The underlying mechanism of MIDY is thought to involve abnormal interactions of misfolded mutant PI with bystander PI-WT in the ER, impairing the ER export of PI-WT and decreasing production of bioactive mature insulin (8,9). However, to date, how these interactions are initiated remains largely unknown. Interestingly, the clinical spectrum of MIDY ranges from neonatal-onset severe insulin-deficient diabetes to relatively late-onset mild diabetes (1,2), suggesting that different PI mutants may behave differently in their folding processes as well as in their ability to interact and obstruct bystander PI-WT in the ER.

In this study, we report that a proline (Pro) substitution for tyrosine residue at the 16th position of the PI B-chain tyrosine-16 (Tyr-B16) [i.e., PI-Y(B16)P] results in dramatic PI misfolding in the ER. Yet, it is unable to interact with bystander PI-WT in the ER and is unable to impair the ER export of PI-WT or to block its ability to form mature insulin. Interestingly, Y(B16)P disrupts the main α-helix

[1]Division of Metabolism, Endocrinology and Diabetes, University of Michigan Medical School, Ann Arbor, MI
[2]Department of Endocrinology and Metabolism, Tianjin Medical University General Hospital, Tianjin, China
[3]Beijing Institute of Pharmacology and Toxicology, Beijing, China
[4]Development, Aging and Regeneration Program, Sanford Burnham Prebys Medical Discovery Institute, La Jolla, CA
[5]Department of Biochemistry and Molecular Biology, Indiana University School of Medicine, Indianapolis, IN
[6]Department of Biochemistry, Case Western Reserve University, Cleveland, OH
[7]Department of Pediatrics, University of California, San Diego, La Jolla, CA
[8]Degenerative Diseases Program, Sanford Burnham Prebys Medical Discovery Institute, La Jolla, CA
[9]Department of Pathology, Immunology and Laboratory Medicine, University of Florida College of Medicine, Gainesville, FL

Corresponding author: Ming Liu, mingliu@tmu.edu.cn, or Peter Arvan, parvan@umich.edu

Received 6 November 2019 and accepted 22 February 2020

This article contains Supplementary Data online at https://diabetes.diabetesjournals.org/lookup/suppl/doi:10.2337/db19-1106/-/DC1.

J.S. and Y.X. contributed equally to this work.

in the PI B-domain. Normally, PI uses this B-domain α-helix in order to homodimerize in the ER (10). Thus, we hypothesize that cross-dimerization between MIDY mutant and PI-WT may be required to initiate their abnormal interaction that impairs the intracellular transport of PI-WT, resulting in insulin deficiency that leads to diabetes (11).

Structural evidence strongly implicates Tyr-B16 as a key residue for normal PI dimerization (12). With this in mind, we have mutagenized this residue to either aspartic acid [Y(B16D)] or alanine [Y(B16)A]; both substitutions were entirely innocuous when introduced into PI-WT. Notably, however, when these substitutions were introduced into the MIDY-causing *Akita* PI-C(A7)Y, each could function as an intra-allelic suppressor, limiting abnormal interactions with PI-WT; alleviating dominant-negative behavior on PI-WT intracellular trafficking; and increasing insulin production in pancreatic β-cell lines and human islets. This study provides insight that protecting the PI-PI contact surface might be a potential druggable target to limit abnormal PI interactions and prevent/delay the development and progression of MIDY.

RESEARCH DESIGN AND METHODS

Materials

Guinea pig polyclonal antiporcine insulin, human insulin-specific radioimmunoassay (RIA) kit, human PI-specific RIA kit, and mouse insulin ELISA kit were from Millipore (Billerica, MA). Guinea pig polyclonal anti-human insulin was from Novus (Centennial, CO). Rabbit polyclonal anti-mouse PI C-peptide (EVEDPQVAQLELGGGPGAGDLQTLA LEVAQQ) was raised by Bioworld (Nanjing, China). Mouse monoclonal anti-human PI C-peptide–A-chain junction (GSLQKRGIVE) was raised by Abmart (Shanghai, China) as previously described (13). Rabbit anti-Myc and anti-GFP were from Immunology Consultants Laboratories (Portland, OR). Rabbit anti-BiP was a gift from Dr. P.S. Kim (U. Cincinnati). The ^{35}S-amino acid mixture was from PerkinElmer (Waltham, MA). Dithiothreitol, protein A-agarose, digitonin, N-ethylmaleimide, brefeldin A, and all other chemical reagents were from Sigma-Aldrich (St. Louis, MO). The 4–12% gradient SDS-PAGE used NuPage gels, and Met/Cys-deficient DMEM and all other tissue culture reagents were from Invitrogen (Thermo Fisher, Waltham, MA). Tris-tricine-urea-SDS-PAGE was performed as described previously (14).

Synthesis and Purification of Single-Chain Insulin Analogs and ^{1}H–Nuclear Magnetic Resonance

Single-chain Tyr^{B16}-DesDi and Asp^{B16}-DesDi insulin analogs were synthesized using a Tribute Peptide Synthesizer with preprogrammed solid-phase Fmoc protocol (15). The synthesis was carried out on a 0.1-mmol scale using H-Asn(Trt)-HMPB-ChemMatrix resin (0.46 mmol/g loading). Side chain protection was Asn(Trt), Arg(Pbf), Asp(OtBu) Cys(Trt), Gln(Trt), Glu(OtBu), His(Trt), Lys(Boc), Ser(tBu), Thr(tBu), Tyr(tBu). DIC/6-chloro-HOBt in 1:2 dichloromethane/DMF was used for the coupling and 20% piperidine in DMF for N$^{\alpha}$-Fmoc-deprotection. The product peptide was then cleaved from the resin and simultaneously deprotected by subjecting it to trifluoroacetic acid (TFA)/TIPS/water/DODT/anisole (90:2.5:2.5:2.5:2.5 v/v) for 2.5 h at ambient temperature. The crude product was precipitated with ice-cold ether, washed, and dried. For folding, 100-mg Asp^{B16}-DesDi crude polypeptide (corresponding to 18 μmol), cysteine hydrochloride (43 mg, 2 mmol/L), and glycine (270 mg, 20 mmol/L) were placed in a 600-mL glass beaker, and distilled, deionized water was added to a 0.1 mmol/L final concentration. The pH of the solution was adjusted to 10.5, and the reaction was stirred open to the air at 4°C for 16 h. The desired folded product was purified both by preparative high-performance liquid chromatography (HPLC) and by analytical reverse-phase HPLC on a C8 Proto (4.6 × 250 mm) 300 Å, 5 μm, Higgins Analytical Inc. column, using 25–50% Solvent B (0.1% TFA in acetonitrile) in Solvent A (0.1% TFA in water) over 35 min at a flow rate of 1.0 mL/min (1525; Waters). Protein elution was monitored at 215 and 280 nm (2489 absorbance detector; Waters), and masses were confirmed by matrix-assisted laser desorption/ionization-time of flight mass spectrometer (MALDI-TOF). Normal insulin helical structure was confirmed by far-ultraviolet circular dichroism spectra from 190 to 250 nm (16), and normal thermodynamic stability was established by guanidine hydrochloride-induced denaturation (monitored by circular dichroism at 222 nm). ^{1}H–nuclear magnetic resonance (^{1}H–NMR) spectra were acquired on protein solutions (0.5 mg in 300 μL D_2O; direct meter reading pD 7.6) at 25°C using a Bruker AVANCE 700 MHz spectrometer.

Synthesis and Purification of Two-Chain Insulin Analogs and Size-Exclusion Chromatography

The nonstandard amino acid ornithine (Orn) was used at position B29 in place of lysine to preserve the side-chain amino group without susceptibility to tryptic cleavage (16). Two-chain insulin analogs ([Tyr^{B16}, Orn^{B29}] insulin and [Asp^{B16}, Orn^{B29}] insulin) were prepared by trypsin-catalyzed cleavage of human insulin or Asp^{B16}-DesDi single-chain insulins (and purification by reverse-phase HPLC) to generate Des-Octapeptide insulins, followed by tryptic-mediated peptide bond formation between Arg^{B22} and a synthetic octapeptide bearing Orn^{B29} (17,18); The final two-chain products were purified by analytical reverse-phase HPLC with molecular mass verified by MALDI-TOF (4700; Applied Biosystems). Self-association properties of the two insulin analogs were determined using HPLC size-exclusion chromatography in the absence of zinc (16). In brief, insulin analogs were made 0.6 mmol/L in 10 mmol/L Tris-HCl (pH 7.4), 140 mmol/L NaCl and 0.02% sodium azide, and 20 μL were loaded on an Enrich SEC70 column (10 mm × 300 mm with fractionation range 3–70 kDa) and were run in the same buffer. Elution time (Supplementary Fig. 1*A*) was monitored by absorbance at 280 nm.

PI Mutagenesis

The plasmids encoding mouse *Ins2* PI-WT or C(A7)Y, untagged human PI-WT, Myc-tagged human PI-WT or C(A7) mutant, hPro-CpepSfGFP bearing Cys(A7) or the Tyr(A7) mutation were described previously (10,14). These plasmids were used as templates to introduce additional Y(B16)D and Y(B16)A mutations using the QuikChange site-directed mutagenesis kit (Stratagene). All resulting plasmids encoding corresponding PI mutations were confirmed by direct DNA sequencing.

Cell Transfection, Metabolic Labeling, Immunoprecipitation, Coprecipitation, Western Blotting, Luciferase Assay, and Human PI- and Insulin-Specific RIA

HEK293 cells, INS1 cells, or Min6 cells were plated into 6- or 12-well plates 1 day before transfection. A total of 1–2 μg plasmid DNA was transfected using Lipofectamine (Invitrogen). For metabolic labeling, transfected 293T cells or Min6 cells were pulse-labeled with ^{35}S-Met/Cys for 30 min with chase for different times as indicated. The chase media and lysed cells were immunoprecipitated (IP) with anti-insulin or anti-Myc, and analyzed using tris-tricine-urea-SDS PAGE or 4–12% gradient SDS-PAGE under reducing and nonreducing conditions as described previously (14). For coprecipitation (co-IP), the cells were lysed with co-IP buffer containing 100 mmol/L NaCl, 25 mmol/L Tris pH 7.0, 0.1% Triton X-100, 5 mmol/L EDTA, and protease inhibitors mixture. Of the total lysates, 90% were IP with anti-GFP followed by Western blotting with anti-PI antibodies as indicated. The remaining 10% of the total lysates were used to determine expression levels of untagged and GFP-tagged PI. For confocal imaging, INS1 cells transfected to express hPro-CpepSfGFP-WT or mutants were permeabilized with 0.5% Triton X-100, fixed with 3.7% formaldehyde and prepared for indirect immunofluorescence, imaged by confocal fluorescence microscopy. The BiP promoter-driven firefly luciferase assay, human PI-specific RIA, and human insulin-specific RIA were described previously (8).

Viral Transduction of Normal Human Islets

A total of 2500 IEQ human islets (Prodo Laboratories, Aliso Viejo, CA) were transduced with 1.5×10^{11} particles of adenoviruses expressing Myc-tagged murine PI-WT, C(A7)Y, or C(A7)Y/Y(B16)D and were incubated in a humidified incubator at 37°C with 5% CO_2 for 12 h. Media were then changed, and islets were harvested 48 h after transduction. Islets were lysed in a buffer containing 25 mmol/L Tris, 0.15 mol/L NaCl, 1 mmol/L EDTA, 1% NP40, 5% glycerol; pH 7.4 (c-Myc Kit IP Lysis Buffer) and protease inhibitors (# 78425; Thermo Fisher). The lysates were resolved by SDS-PAGE and electrotransfered followed by immunoblotting using primary antibodies to human PI, Myc, and GAPDH, with appropriate peroxidase-conjugated secondary antibodies and enhanced chemiluminescence. For human insulin content, islet lysates were assayed using a human insulin ELISA that does not cross-react with PI (# 10–1132–01; Mercodia), following manufacturer's instructions ($n = 3$ in each sample).

Statistical Analyses

Statistical analyses were carried out by two-tailed Student *t* test (for Fig. 4*B* and *D*) or one-way ANOVA followed by Dunnett multiple comparisons (for Fig. 2*B*, *D*, *F*, and *G*, Fig. 5*D*, and Fig. 6*D*–*F*) using GraphPad Prism 7. A *P* value of <0.05 was taken as statistically significant.

Data and Resource Availability

The data sets generated during and/or analyzed during the current study are available from the corresponding author upon reasonable request.

RESULTS

In the ER, PI dimerization (10,19) involves nonpolar association of apposed B-chain residues 8–29 (encompassing the central B9-B19 α-helix), which continue to remain associated in mature insulin (20,21). The insulin crystal structure highlights that B16Y contributes more surface area to the dimerization interface than any other residue (Fig. 1*A* and *B*), and a substitution of this residue yields a high-potency monomeric insulin (12). We therefore engineered both two-chain and single-chain insulin derivatives bearing the Y(B16)D substitution, both of which showed impaired dimerization in dilute solution as judged by size-exclusion chromatography and one-dimensional ^{1}H-NMR spectroscopy, respectively (Fig. 1*C* and *D*). To determine the role of Tyr-B16 in PI folding and dimerization in the ER, we expressed PI-Y(B16)D and Y(B16)A in both 293T and Min6 β-cells. We demonstrated that these substitutions affect neither PI ER oxidative folding (Fig. 2*A*, *B*, *E*, and *F*) nor ER export (Fig. 2*C*–*E* and *G*), suggesting that impaired dimerization alone does prevent the intracellular trafficking of PI. However, Y(B16)P that disrupted the PI B9-B19 α-helix indeed impaired formation of proper disulfide bonds and blocked secretion of PI (Fig. 2), suggesting that the central α-helix of the PI B-chain indeed plays an important role in PI folding in the ER.

We hypothesize that the PI-PI contact surface initiates the attack by misfolded MIDY PI mutants on coexpressed PI-WT. We therefore decided to explore the role of PI-Y(B16) in the interactions between the MIDY-causing *Akita* PI-C(A7)Y and PI-WT. In 293 cells, we coexpressed untagged human PI-WT with Myc-tagged human PI-WT or C(A7)Y [Myc-PI-C(A7)Y] with or without Y(B16)D substitution (Fig. 3*A*, lanes 4–6 and 4′-6′). By nonreducing SDS-PAGE and anti-PI immunoblotting, the overexpression of either untagged PI-WT or Myc-PI-WT resulted in detectable formation of homotypic disulfide-linked complexes (Fig. 3*A*, lanes 2 and 3). Recent evidence indicates that *Akita* PI is similarly predisposed to form a ladder of aberrant disulfide-linked complexes even at low expression levels (13,22,23), and *Akita* PI can heterotypically corecruit PI-WT into these aberrant complexes (9).

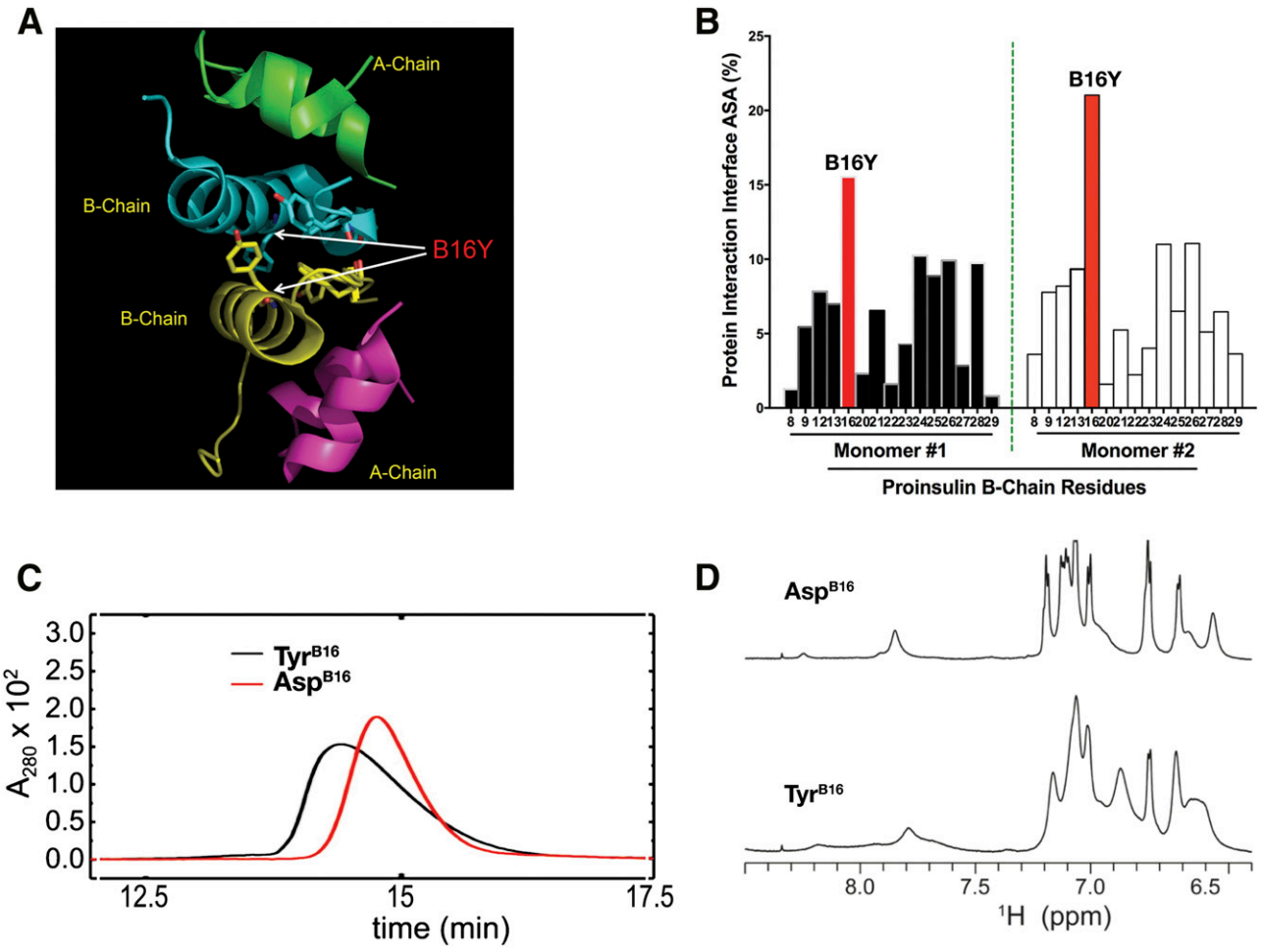

Figure 1— PI Tyr-B16 plays an important role in PI dimerization. *A*: Ribbon-and-stick diagram showing the insulin dimer with the aromatic side chain of B-chain Tyr-16 near the center of the homodimerization surface. *B*: Residues contributing to the accessible surface area (ASA) at the site of contact between two insulin molecules (B-chain residues B9-B29) were identified from the insulin crystal structure using the Protein-Protein Interaction Server. *C*: Two-chain insulin analogs bearing either Tyr-B16 (black line) or AspB16 (red line) were synthesized (see RESEARCH DESIGN AND METHODS), and retention times from 0.6 mmol/L solutions were measured in a zinc-free buffer by size-exclusion chromatography. The data indicate that the AspB16 analog forms at least three times more monomer than the Tyr-B16 analog. *D*: Single-chain Tyr^{B16}-DesDi insulin analog or Asp^{B16}-DesDi insulin analog were synthesized (49 residues, see RESEARCH DESIGN AND METHODS). The aromatic region from one-dimensional ^{1}H–NMR spectra at 700 MHz and 25°C reveals resonance broadening due to self-association of Tyr^{B16}-DesDi single-chain insulin analog (bottom), which is notably mitigated in the Asp^{B16}-DesDi single-chain insulin analog (top).

Upon coexpression, although monomeric forms of Myc-PI-WT, C(A7)Y, and C(A7)Y/Y(B16)D were expressed at comparable levels, Myc-PI-C(A7)Y clearly formed more disulfide-linked dimers (untagged PI dimers and Myc-tagged dimers were marked as D and D′, respectively), heterodimers (marked as H), and higher-molecular-weight PI complexes (Fig. 3*A*, compare lanes 4 and 5). Upon treatment with the reducing agent dithiothreitol, all of these complexes collapsed into a single band of reduced untagged or Myc-tagged-PI, indicating that the bands seen upon nonreducing SDS-PAGE are disulfide-mediated PI dimers and cross-dimers, as well as disulfide-linked PI complexes (DLPCs). Importantly, the formation of these abnormal PI complexes was notably decreased in cells expressing the C(A7)Y/Y(B16)D double mutant (Fig. 3*A*, compare lanes 5 and 6).

To examine whether these disulfide-mediated PI interactions occur in β-cells, we expressed Myc-PI-WT or mutants in Min6 β-cells. As shown in Fig. 3*B*, Myc-PI-C(A7)Y not only formed significantly more abnormal disulfide-linked PI dimers (marked as D′) compared with that of Myc-PI-WT, but also formed disulfide-linked cross-dimers with endogenous PI (noted by an arrow). The high-molecular-weight DLPC were also increased in the cells expressing Myc-PI-C(A7)Y (Fig. 3*B*, compare lanes 2 and 3). However, once again, introducing the intra-allelic Y(B16)D significantly decreased these abnormal PI complexes (Fig. 3*B*, compare lanes 3 and 4). Together, these results suggest that limiting PI-PI interactions by introducing Y(B16)D can decrease formation of abnormal DLPCs between PI-C(A7)Y and PI-WT.

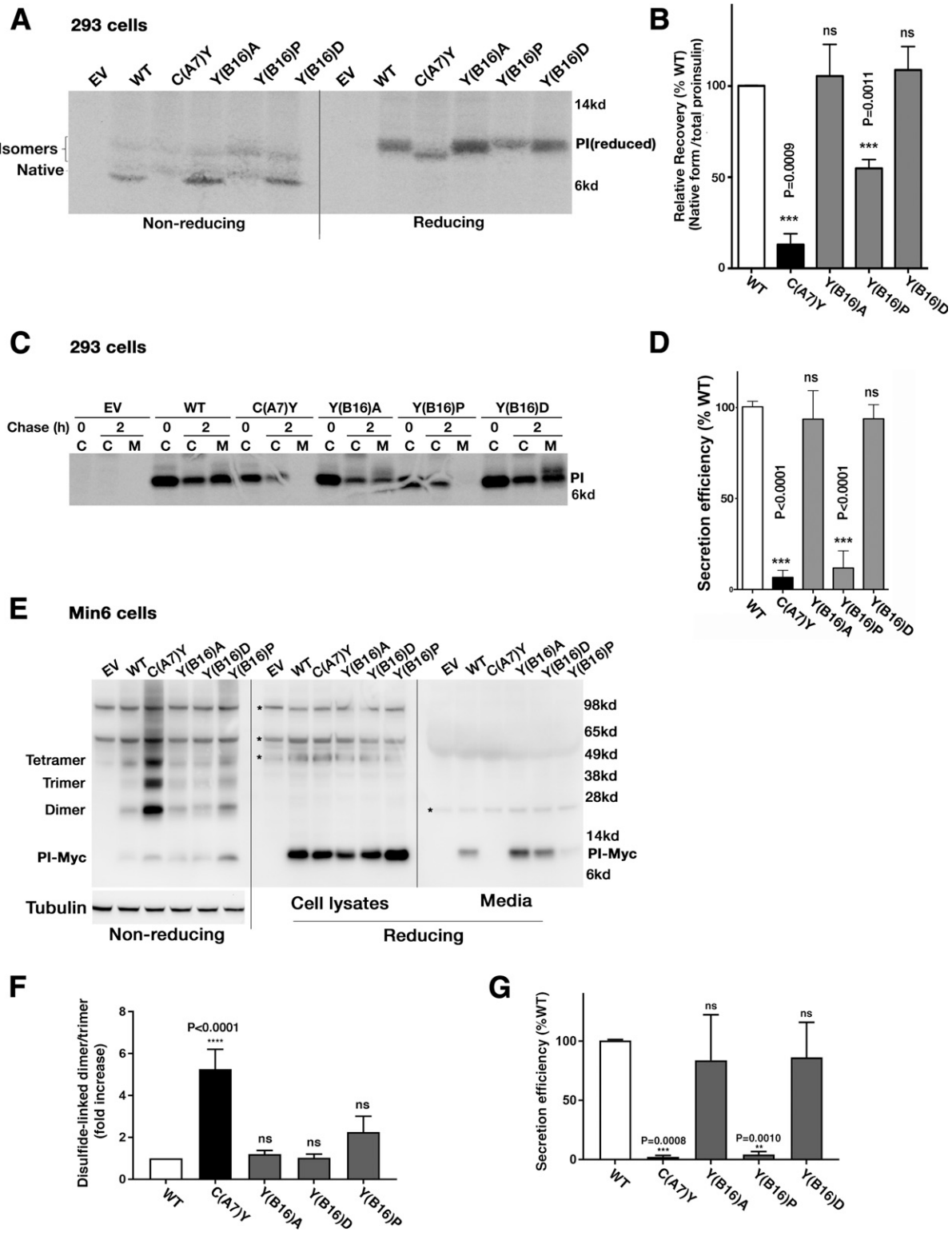

Figure 2—Asp (D) or Ala (A), but not Pro (P), substitution at PI Tyr-B16 does not affect folding and secretion of PI. *A* and *B*: 293 cells transfected with empty vector (EV) or plasmids encoding PI-WT, C(A7)Y, Y(B16)A, Y(B16)D, or Y(B16)P were metabolic labeled for 30 min without chase. The newly synthesized PI was IP by anti-insulin followed by analysis of tris-tricine-urea-SDS-PAGE under both nonreducing and reducing conditions. Native PI with correct disulfide pairing recovered under nonreducing conditions as well as total synthesized PI recovered under reducing conditions were quantified and analyzed in *B* ($n = 3$). The relative recovery of native PI in the cells expressing PI-WT was set to 100%. *C*: 293 cells transfected with plasmids encoding PI-WT, C(A7)Y, Y(B16)A, Y(B16)D, or Y(B16)P were metabolic labeled for 30 min followed by 0 or 2 h chase as indicated. The chase media (M) were collected and cells (C) were lysed. Biosynthesis and secretion of mutant PIs were analyzed by IP with anti-insulin followed by 4–12% NuPage. *D*: The results from *C* ($n = 3$) were quantified; the secretion efficiency of PI-WT and mutants was calculated, and that of PI-WT was set to 100%. *E*: Min6 cells were transiently transfected to express Myc-tagged PI-WT or mutants as indicated. Misfolded DLPCs in the cell lysates analyzed by 4–12% NuPage under both reducing and

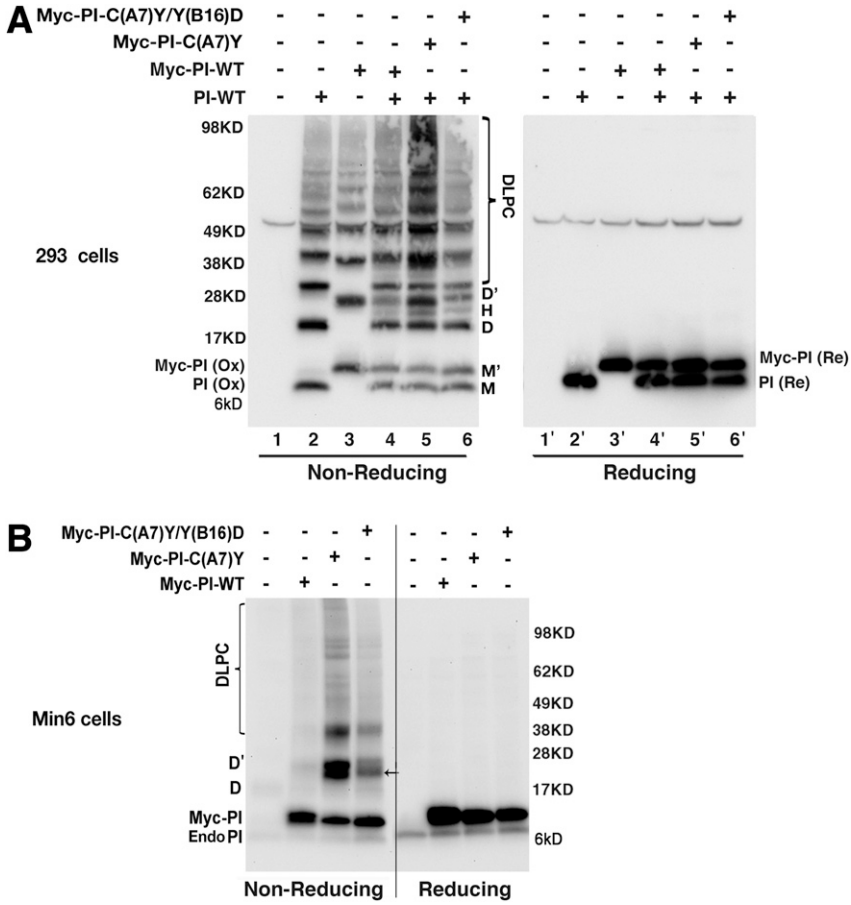

Figure 3—Substitution of Tyr with Asp at PI B16 limits formation of heterodimerization and DLPCs. *A*: 293 cells were transfected with plasmids encoding untagged PI-WT, Myc-PI-WT, or PI mutants as indicated. Oxidative (Ox) folding, disulfide-linked PI dimers, and high-molecular-weight DLPCs were analyzed under nonreducing condition (left panel). Total amount of PI-WT and Myc-PI-WT or mutants were analyzed under reducing (Re) condition (right panel). *B*: Min6 cells were transfected with plasmids encoding Myc-tagged PI-WT or mutants as indicated. Oxidative folding of PI-WT and mutants were analyzed under nonreducing conditions (left panel). The heterodimer formed by Myc-tagged PI-mutant with endogenous PI is indicated by the arrow. The total amount of Myc-tagged PI-WT and mutants were analyzed under reducing condition (right panel). D, homo-dimers formed by untagged PI; D′ refers to homo-dimers formed by Myc-PI; H, hetero-dimers formed by untagged PI with Myc-PI.

To further confirm this point, we expressed GFP-tagged PI-C(A7)Y with or without the Y(B16)D substitution in both 293 cells and Min6 cells. We found that Y(B16)D inhibits co-IP of PI-WT by GFP-PI-C(A7)Y in both 293 cells (Fig. 4*A* and *B*) and Min6 cells (Fig. 4*C* and *D*) under steady-state condition. Thus, the Y(B16)D substitution decreases the strength of interaction of MIDY PI with PI-WT in the ER.

Next, we examined folding and secretion of PI-C(A7)Y with or without B16 substitutions, and we found that the introduction of Asp (D), Ala (A), or Pro (P) had no effect on the impaired disulfide maturation of PI-C(A7)Y, and did not rescue secretion of the MIDY mutant (which was retained intracellularly) in both 293 cells (Fig. 5*A* and *B*) and Min6 cells (Fig. 5*C*). We then checked whether B16 substitutions could limit the dominant-negative effect of PI-C(A7)Y on bystander PI-WT. We coexpressed mouse PI-C(A7)Y ± Y(B16)D or Y(B16)P substitutions with human PI-WT in 293T cells. We used a species-specific immunoassay to follow the secretion of coexpressed human PI-WT in the presence of mutant PI. Indeed, the expression of mouse PI-C(A7)Y blocked the secretion of

nonreducing conditions (left and middle panels). The media were incubated overnight and were used to analyzed secretion efficiency of PI-WT and mutants (right panel). *Refers to nonspecific bands. *F*: In three independent experiments shown in *E*, the disulfide-linked dimer and trimer under nonreducing condition and total PI-WT or mutants under reducing condition were quantified. The ratios (dimer + trimer/total PI) were calculated and that of PI-WT was set to 1. *G*: The secretion efficiency (media/cell lysates) of PI-WT and mutants from three independent experiments shown in *E* was calculated, and that of the PI-WT was set to 100%. ns, not significant.

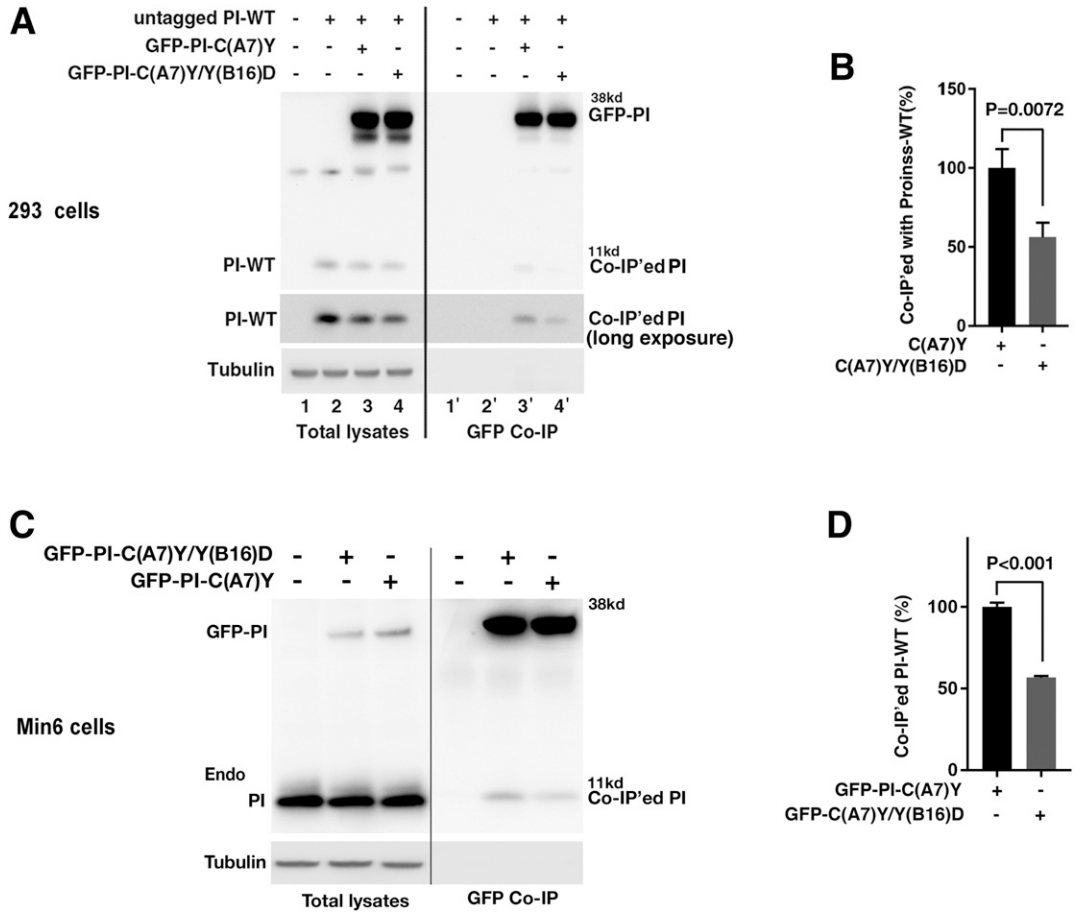

Figure 4—Substitution of Tyr with Asp at PI B16 limits abnormal interactions between WT PI and diabetes causing C(A7)Y mutant PI. *A*: 293 cells were cotransfected with plasmids encoding untagged PI-WT, or GFP-tagged PI bearing the C(A7)Y mutation [GFP-PI-C(A7)Y], or GFP-tagged PI bearing both the C(A7)Y mutation as well as an intragenic suppressor mutation, Y(B16)D [GFP-PI-C(A7)Y/Y(B16)D] at a DNA ratio of 1:1. At 48 h after transfection, the cells were lysed in a co-IP buffer; 90% of the total lysates were IP with anti-GFP. IP GFP-PI and co-IP PI-WT were resolved in 4–12% NuPage under reducing condition along with 10% of the total lysates, transferred to the nitrocellulose membrane, and blotted with anti-human PI, which can recognize both untagged human PI and GFP-PI. *B*: The co-IP PI-WT and that in the total lysates were quantified using Image J. The percent of co-IP PI-WT in the total lysates was calculated and that of co-IP by GFP-PI-C(A7)Y set as 100%. *C*: Min6 cells transfected with plasmids encoding GFP-PI-C(A7)Y or GFP-PI-C(A7)Y/Y(B16)D were lysed in a co-IP buffer and IP with anti-GFP. The endogenous PI in the total lysates and co-IP with anti-GFP were resolved in 4–12% NuPage under reducing condition, transferred to the nitrocellulose membrane, and blotted with anti-mouse PI, which can recognize both endogenous mouse PI and GFP-PI. *D*: The co-IP endogenous PI and that in the total lysates were quantified using Image J. The percent of co-IP endogenous PI in the total lysates was calculated and that of co-IP by GFP-PI-C(A7)Y set as 100%.

PI-WT by ~70% (Fig. 5*D*), which is consistent with previous reports (8,9,14,24). However, the Y(B16)D substitution [or Y(B16)P] functioned as an intra-allelic suppressor of the dominant-negative effect of PI-C(A7)Y on the secretion of coexpressed PI-WT (Fig. 5*D*).

These immunoassay results were then confirmed using pulse-chase experiments. Once again, PI-Y(B16)A and PI-Y(B16)D were secreted normally, in parallel with the secretion of coexpressed PI-WT (Fig. 5*E*, lanes 15 or 21). Further, both misfolded mutants PI-C(A7)Y and PI-Y(B16)P were fully blocked in their secretion. However, the *Akita* PI-C(A7)Y conferred a clear dominant-negative effect on coexpressed PI-WT that was not apparent for PI-Y(B16)P (Fig. 5*E*, lanes 12 vs. 18), indicating that not all misfolded PI mutants have the ability to block secretion of bystander PI-WT. Moreover, we found that neither PI-C(A7)Y/Y(B16)A nor C(A7)Y/Y(B16)D could block the secretion of coexpressed PI-WT (Fig. 5*E*, lanes 12 vs. 24 or 30), indicating that these Tyr-B16 substitutions reversed the dominant-negative effect of *Akita* mutant PI.

To further investigate the effect of B16 substitutions on endogenous PI in β-cells, we transfected GFP-tagged PI-WT or mutants, and we used three independent approaches to examine transdominant effects. First, using confocal immunofluorescence, we found that while GFP-PI-WT and Y(B16)D showed a punctate insulin secretory granule pattern, PI-C(A7)Y appeared in a typical ER pattern and caused a profound loss of endogenous insulin (Fig. 6*A* middle, white arrows). However, although the double mutant PI-C(A7)Y/Y(B16)D also appeared to be

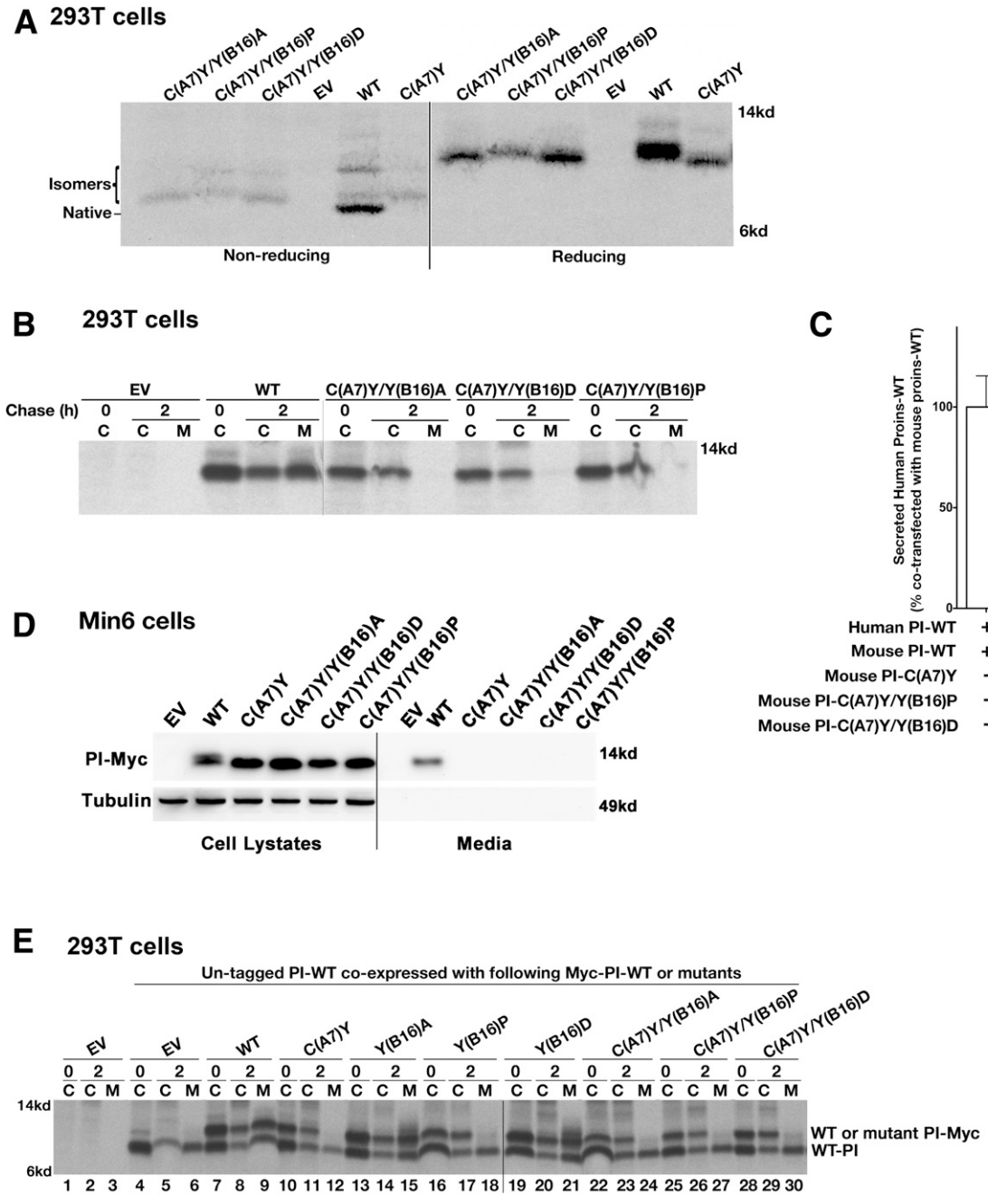

Figure 5—Mutations at PI B16 do not improve folding of diabetes causing PI-C(A7)Y but alleviate its transdominant-negative effect on coexpressed PI-WT. *A*: 293 cells cotransfected with indicated plasmids were labeled with ^{35}Met/Cys for 30 min without chase. Biosynthesis and folding of newly synthesized PI-WT and mutants were analyzed by tris-tricine-urea-SDS-PAGE under both nonreducing and reducing conditions. *B*: 293 cells transfected and pulse-labeled as in *A* were chased 0 or 2 h. The chase media (M) were collected and cells (C) were lysed and analyzed by IP with anti-insulin followed by 4–12% NuPage under reducing conditions. *C*: Min6 cells were transfected with plasmids encoding Myc-tagged PI-WT or mutants as indicated. At 48 h after transfection, the media, which were cultured overnight, were collected, and the cells were lysed. The secretion efficiency of PI-WT and mutants was analyzed by Western blotting using anti-Myc. *D*: 293 cells were cotransfected with a plasmid encoding human PI-WT (human PI-WT) and either mouse PI-WT (mouse PI-WT) or mutants as indicated. The secretion of human PI-WT in the presence of mouse PI-WT or mutants was measured using human PI-specific RIA (mean ± SD, $n = 3$). *E*: 293 cells were cotransfected with a plasmid encoding untagged PI-WT and Myc-tagged PI-WT or mutants as indicated. At 48 h after transfection, the cells were labeled with ^{35}Met/Cys for 30 min with 0 or 2 h chase. The cell lysates and chase media were collected and IP with anti-insulin. The secretion efficiency of untagged PI-WT in the presence or absence of Myc-PI-WT or mutants were analyzed under reducing conditions. proins, proinsulin.

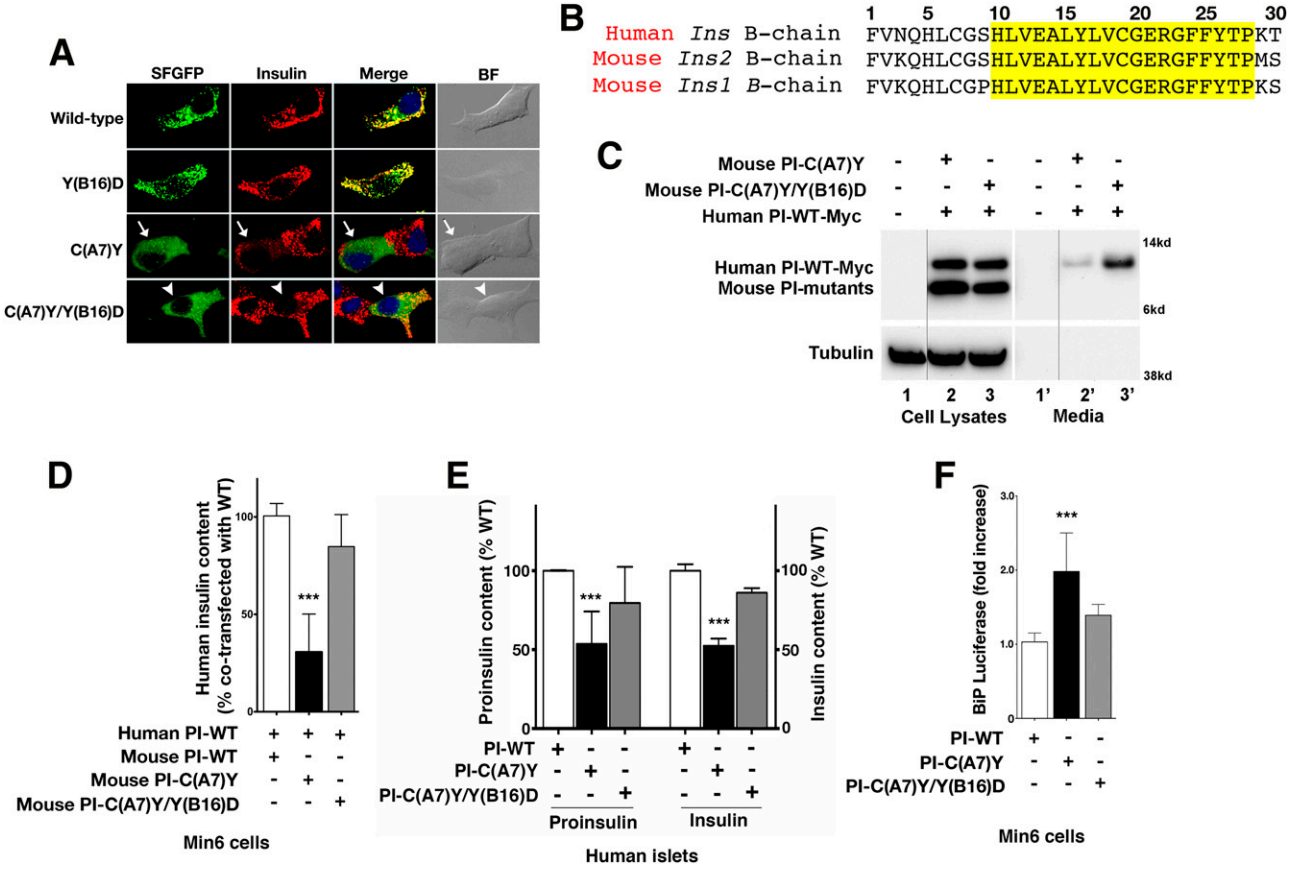

Figure 6—PI B16 mutations function as an intragenic suppressor of the dominant-negative effects of MIDY PI-C(A7)Y and alleviate β-cell ER stress. *A*: INS1 cells were transfected with plasmids encoding GFP-tagged PI-WT and mutants as indicated. At 48 h after transfection, the cells were fixed and permeabilized. Confocal immunofluorescence microscopy was performed after double-labeling with anti-GFP (green) and anti-insulin (red). Whereas the cells expressing GFP-C(A7)Y exhibited a diminution of endogenous insulin staining (middle panels, white arrows), in the cells expressing a GFP-C(A7)Y/Y(B16)D endogenous insulin was restored (bottom panels, white arrowheads). *B*: The 30 residues of the B-chain of human PI, mouse PI 2 (*Ins2*), and mouse PI 1 (*Ins1*) were aligned. The highly conserved domain (B10-B28) that are involved PI dimerization is highlighted in yellow. *C*: 293 cells were cotransfected with plasmids encoding Myc-tagged human PI-WT with untagged mouse mutants. The media were cultured overnight and were collected at 48 h after transfection. Secretion of Myc-tagged human PI-WT in the presence of untagged mouse PI mutants was examined by Western blotting using anti-PI. *D*: Min6 cells were cotransfected with plasmids encoding human PI-WT with either mouse PI-WT or mutants at a DNA ratio of 1:3. At 48 h after transfection, human insulin content in the transfected cells was measured using human insulin-specific RIA (mean ± SD, $n = 3$). ***$P < 0.0001$ comparing the human insulin content in the cells expressing mouse PI-C(A7)Y with that of PI-WT and PI-C(A7)Y/Y(B16)D. *E*: Human islets were transduced with adenoviruses expressing Myc-tagged mouse PI-WT, C(A7)Y, or C(A7)Y/Y(B16)D, as indicated. At 48 h after infection, human insulin content in the infected human islets was measured by human insulin-specific ELISA. Human PI content was measured by densitometry of Western blotting. The relative contents of human PI and insulin in human islets infected with mouse PI-WT were set to 100%. ***P values comparing the human PI content ($P = 0.0023$) and human insulin content ($P = 0.0004$), respectively, in the islets infected with mouse PI-C(A7)Y with that of infected with PI-WT. *F*: Min6 cells were triple-transfected with plasmids encoding firefly luciferase driven by a BiP promoter, cytomegalovirus-renilla luciferase, and either PI-WT or mutants at a DNA ratio of 1:2:4. At 48 h after transfection, luciferase activities in transfected cells were measured as described in RESEARCH DESIGN AND METHODS (mean ± SD, $n = 4$). ***$P < 0.0001$ comparing BiP luciferase in the cells expressing PI-C(A7)Y with that of expressing PI-WT.

retained in the ER, it did not detectably decrease endogenous insulin in β-cells (Fig. 6*A* bottom, white arrowheads). Second, using human insulin-specific RIA, we confirmed that introducing Y(B16)D in PI-C(A7)Y alleviated the transdominant effect of the MIDY mutant as demonstrated by increased insulin production (Fig. 6*B*). Further, in human islets, adenoviral expression of mouse PI-C(A7)Y significantly decreased human PI and insulin content, whereas comparable expression of the C(A7)Y/Y(B16)D mutant (Supplementary Fig. 3) again demonstrated intra-allelic suppression of the dominant-negative effect of the MIDY mutant on both human PI and insulin (Fig. 6*D*). Finally, the enhanced ER export of PI-WT correlated with decreased ER stress in β-cells coexpressing PI-C(A7)Y versus C(A7)Y/Y(B16)D, as measured in a transcriptional BiP promoter reporter assay (Fig. 6*D*). Taken together, these results strongly suggest that Tyr-B16, which is a major component of the PI-PI interaction surface, is involved in the physical interaction between MIDY mutant PI and PI-WT, and this interaction is necessary for

the mutant protein to block PI-WT exit from the ER, impair insulin production, trigger ER stress, and promote the development of diabetes.

DISCUSSION

To date, more than 50 insulin gene mutations have been reported to cause MIDY, an autosomal-dominant form of diabetes (also known as maturity-onset diabetes of the young type 10) (1,11). More than 60% of the identified mutant alleles have been predicted or experimentally confirmed to impair oxidative folding of PI in the ER (1,25). Importantly, these misfolded MIDY mutants not only fail to exit from the ER, but also physically attack coexpressed PI-WT, impairing the folding and ER export of coexpressed PI-WT, decreasing insulin production, and initiating insulin-deficient diabetes (11,14,26). Heretofore, the molecular mechanism underlying these dominant-negative effects have been completely unknown. As the PI-PI contact surface might possibly engage even before completion of the folding of individual PI monomers, the present work focuses attention on this surface as a possible site initiating the attack of misfolded mutant PI onto bystander PI in the ER.

In this study, we found at least two substitutions of the key Tyr-B16 residue that had no observable impact on PI monomer folding or ER export but that could limit PI-PI contact and thereby decrease abnormal interactions and alleviate transdominant effects of observed in MIDY. It is interesting to note that among the roughly 30 known PI sites/residues that trigger MIDY, none has yet been described that introduces a charged or highly polar residue into the B9-B19 α-helix. We postulate that such substitutions may be relatively ineffective in propagating misfolding onto bystander PI-WT molecules. This hypothesis is supported by data from the PI-Y(B16)P mutant, which disrupts the B9-B19 α-helix to cause severe PI misfolding and ER retention (Fig. 1), but it cannot impose a dominant-negative effect on bystander PI-WT (Fig. 5). These data support the notion that PI-PI contact is an early folding event and initiates the transdominant effects of MIDY mutants.

Increasing evidence indicates that PI misfolding and ER stress not only are the molecular basis of MIDY but may also play an important role in the development and progression of type 1 and type 2 diabetes (2,27–30). Increased PI misfolding has been recently reported in β-cells with either defects in the ER folding environment (31–33), defective ER export machinery (13), or increased PI synthesis due to insulin resistance in rodent and human type 2 diabetes islets (23). These data suggest that PI misfolding is an early event in the progression to type 2 diabetes. As the most abundant protein synthesized in β-cells, PI is predisposed to misfold (11,14,34) from which it may propagate this misfolding onto bystander PI (1,8,9). This becomes an important driving force for β-cell ER stress and insulin deficiency (32,35–37). The data in this report provide the first evidence pointing to the idea that initial PI-PI B-chain contact may be a site worth targeting, to block cross-dimerization of misfolded PI with PI bystanders, enhance insulin production, and offer a new approach to preventing β-cell insulin deficiency and diabetes (Fig. 7).

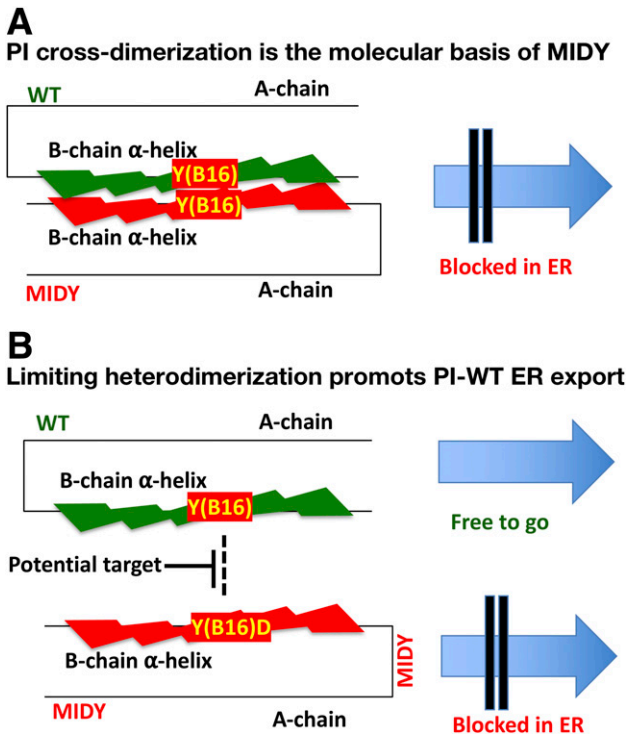

Figure 7—A working model of misfolded mutant PI attacking the dimerization surface of bystander PI-WT as a control point for PI ER export and insulin production. *A*: PI forms dimers in the ER. In the β-cells that coexpress PI-WT (blue) and misfolded mutant PI (red), the PI dimerization surface of the mutant can abnormally interact with that of the coexpressed bystander PI-WT, which impairs the folding and the ER export of PI-WT. *B*: Protecting the PI dimerization surface may serve as a potential theropeutic target to limit transdominant effects of misfolded mutant PI, alleviating ER stress and β-cell failure.

Acknowledgments. The authors thank Nelson Phillips at Case Western Reserve University for advice regarding size-exclusion chromatography.

Funding. This work was supported by National Institutes of Health (NIH) (R01-DK-48280, R24-DK-110973, DK-111174, and R01-DK-040949), Natural Science Foundation of China (81830025, 81620108004, and 81570699), and National Key R&D Program of China (2019YFA0802502). We acknowledge support from Tianjin Municipal Science and Technology Commission (17ZXMFSY00150), from the Michigan Diabetes Research Center Morphology Core (NIH P30-DK-020572), and from the Protein Folding Diseases Initiative of the University of Michigan. Human pancreatic islets were provided by the National Institute of Diabetes and Digestive and Kidney Diseases–funded Integrated Islet Distribution Program (IIDP) at City of Hope (NIH 2UC4-DK-098085) and JDRF-funded IIDP Islet Award Initiative. N.R. is a Predoctoral Fellow of the NIH Medical Scientist Training Program at Case Western Reserve University (5T32GM007250-38) supported by an NIH fellowship (1F30-DK-112644).

Duality of Interest. No potential conflicts of interest relevant to this article were reported.

Author Contributions. J.S., Y.X., X.L., L.H., W.C., S.A.M., L.L., R.M., D.L., A.A., B.D., N.R., N.P.W., P.I.-A., and D.A.O. generated research data. M.A.W., P.I.A.,

R.J.K., and D.A.O. contributed to discussion and reviewed/edited the manuscript. P.A. and M.L. initiated and designed the research project, reviewed the data, and wrote the manuscript. M.L. and P.A. are the guarantors of this work and, as such, had full access to all the data in the study and take responsibility for the integrity of the data and the accuracy of the data analysis.

References

1. Liu M, Sun J, Cui J, et al. INS-gene mutations: from genetics and beta cell biology to clinical disease. Mol Aspects Med 2015;42:3–18
2. Liu M, Hodish I, Haataja L, et al. Proinsulin misfolding and diabetes: mutant INS gene-induced diabetes of youth. Trends Endocrinol Metab 2010;21:652–659
3. Colombo C, Porzio O, Liu M, et al.; Early Onset Diabetes Study Group of the Italian Society of Pediatric Endocrinology and Diabetes (SIEDP). Seven mutations in the human insulin gene linked to permanent neonatal/infancy-onset diabetes mellitus. J Clin Invest 2008;118:2148–2156
4. Edghill EL, Flanagan SE, Patch A-M, et al.; Neonatal Diabetes International Collaborative Group. Insulin mutation screening in 1,044 patients with diabetes: mutations in the INS gene are a common cause of neonatal diabetes but a rare cause of diabetes diagnosed in childhood or adulthood. Diabetes 2008;57:1034–1042
5. Støy J, Edghill EL, Flanagan SE, et al.; Neonatal Diabetes International Collaborative Group. Insulin gene mutations as a cause of permanent neonatal diabetes. Proc Natl Acad Sci U S A 2007;104:15040–15044
6. Polak M, Dechaume A, Cavé H, et al.; French ND (Neonatal Diabetes) Study Group. Heterozygous missense mutations in the insulin gene are linked to permanent diabetes appearing in the neonatal period or in early infancy: a report from the French ND (Neonatal Diabetes) Study Group. Diabetes 2008;57:1115–1119
7. Garin I, Edghill EL, Akerman I, et al.; Neonatal Diabetes International Group. Recessive mutations in the INS gene result in neonatal diabetes through reduced insulin biosynthesis. Proc Natl Acad Sci U S A 2010;107:3105–3110
8. Liu M, Haataja L, Wright J, et al. Mutant INS-gene induced diabetes of youth: proinsulin cysteine residues impose dominant-negative inhibition on wild-type proinsulin transport. PLoS One 2010;5:e13333
9. Liu M, Hodish I, Rhodes CJ, Arvan P. Proinsulin maturation, misfolding, and proteotoxicity. Proc Natl Acad Sci U S A 2007;104:15841–15846
10. Haataja L, Snapp E, Wright J, et al. Proinsulin intermolecular interactions during secretory trafficking in pancreatic β cells. J Biol Chem 2013;288:1896–1906
11. Liu M, Weiss MA, Arunagiri A, et al. Biosynthesis, structure, and folding of the insulin precursor protein. Diabetes Obes Metab 2018;20(Suppl. 2):28–50
12. Ludvigsen S, Roy M, Thøgersen H, Kaarsholm NC. High-resolution structure of an engineered biologically potent insulin monomer, B16 Tyr–>His, as determined by nuclear magnetic resonance spectroscopy. Biochemistry 1994;33:7998–8006
13. Zhu R, Li X, Xu J, et al. Defective endoplasmic reticulum export causes proinsulin misfolding in pancreatic β cells. Mol Cell Endocrinol 2019;493:110470
14. Liu M, Lara-Lemus R, Shan SO, et al. Impaired cleavage of preproinsulin signal peptide linked to autosomal-dominant diabetes. Diabetes 2012;61:828–837
15. Zaykov AN, Mayer JP, Gelfanov VM, DiMarchi RD. Chemical synthesis of insulin analogs through a novel precursor. ACS Chem Biol 2014;9:683–691
16. Pandyarajan V, Phillips NB, Rege N, Lawrence MC, Whittaker J, Weiss MA. Contribution of TyrB26 to the function and stability of insulin: structure-activity relationships at a conserved hormone-receptor interface. J Biol Chem 2016;291:12978–12990
17. Kubiak T, Cowburn D. Enzymatic semisynthesis of porcine despentapeptide (B26-30) insulin using unprotected desoctapeptide (B23-30) insulin as a substrate. Model studies. Int J Pept Protein Res 1986;27:514–521
18. Inouye K, Watanabe K, Tochino Y, Kobayashi M, Shigeta Y. Semisynthesis and properties of some insulin analogs. Biopolymers 1981;20:1845–1858
19. Quinn D, Orci L, Ravazzola M, Moore HP. Intracellular transport and sorting of mutant human proinsulins that fail to form hexamers. J Cell Biol 1991;113:987–996
20. Whittingham JL, Youshang Z, Záková L, et al. *I*222 crystal form of despentapeptide (B26-B30) insulin provides new insights into the properties of monomeric insulin. Acta Crystallogr D Biol Crystallogr 2006;62:505–511
21. Brange J, Ribel U, Hansen JF, et al. Monomeric insulins obtained by protein engineering and their medical implications. Nature 1988;333:679–682
22. Izumi T, Yokota-Hashimoto H, Zhao S, Wang J, Halban PA, Takeuchi T. Dominant negative pathogenesis by mutant proinsulin in the Akita diabetic mouse. Diabetes 2003;52:409–416
23. Arunagiri A, Haataja L, Pottekat A, et al. Proinsulin misfolding is an early event in the progression to type 2 diabetes. eLife 2019;8:e44532
24. Park S-Y, Ye H, Steiner DF, Bell GI. Mutant proinsulin proteins associated with neonatal diabetes are retained in the endoplasmic reticulum and not efficiently secreted. Biochem Biophys Res Commun 2010;391:1449–1454
25. Weiss MA. Diabetes mellitus due to the toxic misfolding of proinsulin variants. FEBS Lett 2013;587:1942–1950
26. Arunagiri A, Haataja L, Cunningham CN, et al. Misfolded proinsulin in the endoplasmic reticulum during development of beta cell failure in diabetes. Ann N Y Acad Sci 2018;1418:5–19
27. Papa FR. Endoplasmic reticulum stress, pancreatic β-cell degeneration, and diabetes. Cold Spring Harb Perspect Med 2012;2:a007666
28. Tersey SA, Nishiki Y, Templin AT, et al. Islet β-cell endoplasmic reticulum stress precedes the onset of type 1 diabetes in the nonobese diabetic mouse model. Diabetes 2012;61:818–827
29. Scheuner D, Kaufman RJ. The unfolded protein response: a pathway that links insulin demand with beta-cell failure and diabetes. Endocr Rev 2008;29:317–333
30. Riahi Y, Israeli T, Cerasi E, Leibowitz G. Effects of proinsulin misfolding on β-cell dynamics, differentiation and function in diabetes. Diabetes Obes Metab 2018;20(Suppl. 2):95–103
31. Tsuchiya Y, Saito M, Kadokura H, et al. IRE1-XBP1 pathway regulates oxidative proinsulin folding in pancreatic β cells. J Cell Biol 2018;217:1287–1301
32. Zito E, Chin KT, Blais J, Harding HP, Ron D. ERO1-beta, a pancreas-specific disulfide oxidase, promotes insulin biogenesis and glucose homeostasis. J Cell Biol 2010;188:821–832
33. Jang I, Pottekat A, Poothong J, et al. PDIA1/P4HB is required for efficient proinsulin maturation and ß cell health in response to diet induced obesity. eLife 2019;8:e44528
34. Guo H, Xiong Y, Witkowski P, et al. Inefficient translocation of preproinsulin contributes to pancreatic β cell failure and late-onset diabetes. J Biol Chem 2014;289:16290–16302
35. Wang J, Chen Y, Yuan Q, Tang W, Zhang X, Osei K. Control of precursor maturation and disposal is an early regulative mechanism in the normal insulin production of pancreatic β-cells. PLoS One 2011;6:e19446
36. Sun J, Cui J, He Q, Chen Z, Arvan P, Liu M. Proinsulin misfolding and endoplasmic reticulum stress during the development and progression of diabetes. Mol Aspects Med 2015;42:105–118
37. Liu M, Li Y, Cavener D, Arvan P. Proinsulin disulfide maturation and misfolding in the endoplasmic reticulum. J Biol Chem 2005;280:13209–13212